

# Scalar Top Quark Studies with Various Visible Energies

A. Sopczak<sup>1</sup>, M. Carena<sup>2</sup>, A. Finch<sup>1</sup>, A. Freitas<sup>2</sup>,  
C. Milstène<sup>2</sup>, H. Nowak<sup>3</sup>

<sup>(1)</sup>Lancaster University, UK, <sup>(2)</sup>Fermilab, USA, <sup>(3)</sup>DESY Zeuthen, Germany.

## Abstract

The precision determination of scalar top quark properties will play an important rôle at a future International Linear Collider (ILC). Recent and ongoing studies are discussed for different experimental topologies in the detector. First results are presented for small mass differences between the scalar top and neutralino masses. This corresponds to a small expected visible energy in the detector. An ILC will be a unique accelerator to explore this scenario. In addition to finding the existence of light stop quarks, the precise measurement of their properties is crucial for testing their impact on the dark matter relic abundance and the mechanism of electroweak baryogenesis. Significant sensitivity for mass differences down to 5 GeV are obtained. The simulation is based on a fast and realistic detector simulation. A vertex detector concept of the Linear Collider Flavor Identification (LCFI) collaboration, which studies pixel detectors for heavy quark flavour identification, is implemented in the simulations for c-quark tagging. The study extends simulations for large mass differences (large visible energy) for which aspects of different detector simulations, the vertex detector design, and different methods for the determination of the scalar top mass are discussed. Based on the detailed simulations we study the uncertainties for the dark matter density predictions and their estimated uncertainties from various sources. In the region of parameters where stop-neutralino co-annihilation leads to a value of the relic density consistent with experimental results, as precisely determined by the Wilkinson Microwave Anisotropy Probe (WMAP), the stop-neutralino mass difference is small and the ILC will be able to explore this region efficiently.

*Presented at the 13th International Conference on Supersymmetry and Unification of Fundamental Interactions (SUSY'05), Durham, UK, July 18-23, 2005.*



# Scalar Top Quark Studies with Various Visible Energies

A. Sopczak<sup>1\*</sup>, M. Carena<sup>2</sup>, A. Finch<sup>1</sup>, A. Freitas<sup>2</sup>, C. Milstène<sup>2</sup>, H. Nowak<sup>3</sup>

(1) *Lancaster University, Lancaster LA1 4YB, United Kingdom,*

(2) *Fermi National Accelerator Laboratory, Batavia, IL 60510-500, USA, and*

(3) *Deutsches Elektronen-Synchrotron DESY, D-15738 Zeuthen, Germany.*

The precision determination of scalar top quark properties will play an important rôle at a future International Linear Collider (ILC). Recent and ongoing studies are discussed for different experimental topologies in the detector. First results are presented for small mass differences between the scalar top and neutralino masses. This corresponds to a small expected visible energy in the detector. An ILC will be a unique accelerator to explore this scenario. In addition to finding the existence of light stop quarks, the precise measurement of their properties is crucial for testing their impact on the dark matter relic abundance and the mechanism of electroweak baryogenesis. Significant sensitivity for mass differences down to 5 GeV are obtained. The simulation is based on a fast and realistic detector simulation. A vertex detector concept of the Linear Collider Flavor Identification (LCFI) collaboration, which studies pixel detectors for heavy quark flavour identification, is implemented in the simulations for c-quark tagging. The study extends simulations for large mass differences (large visible energy) for which aspects of different detector simulations, the vertex detector design, and different methods for the determination of the scalar top mass are discussed. Based on the detailed simulations we study the uncertainties for the dark matter density predictions and their estimated uncertainties from various sources. In the region of parameters where stop-neutralino co-annihilation leads to a value of the relic density consistent with experimental results, as precisely determined by the Wilkinson Microwave Anisotropy Probe (WMAP), the stop-neutralino mass difference is small and the ILC will be able to explore this region efficiently.

## 1. INTRODUCTION

The production and decay of scalar top quarks (stops) is particularly interesting for the development of the vertex detector as only two c-quarks and missing energy (from undetected neutralinos) are produced for light stops. The reaction  $e^+e^- \rightarrow \tilde{t}_1\tilde{t}_1^* \rightarrow c\tilde{\chi}_1^0\bar{c}\tilde{\chi}_1^0$  is shown in Fig. 1.

The study of small mass differences between stop and neutralino is strongly motivated cosmologically. A long history of experimental observations has corroborated the evidence for dark matter in the universe, culminating in the recent accurate determination by the WMAP satellite, in combination with the Sloan Digital Sky Survey (SDSS) [1],  $\Omega_{\text{CDM}}h^2 = 0.1126^{+0.0161}_{-0.0181}$  at the 95% C.L. Here  $\Omega_{\text{CDM}}$  is the dark matter energy density normalized to the critical density and  $h$  is the Hubble parameter in units of 100 km/s/Mpc. Supersymmetry with  $R$ -parity conservation provides a natural dark matter candidate, which in most scenarios is the lightest neutralino.

Electroweak baryogenesis is based on the concept that the baryon asymmetry is generated at the electroweak phase transition. While in the Standard Model the phase transition is not sufficiently strongly first order and there is not enough CP violation, Supersymmetry can alleviate both shortcomings. A strong first-order phase transition can be induced by loop effects of light scalar top quarks (stops) to the Higgs potential. In much of the parameter space of interest for electroweak baryogenesis, the light stop is only slightly heavier than the lightest neutralino, thus implying that stop-neutralino co-annihilation is significant. In the co-annihilation region, the stop-neutralino mass difference is typically smaller than 30 GeV [2], making a discovery of the stops at hadron colliders difficult.

The LCFI Collaboration develops a CCD vertex detector for a future Linear Collider. This vertex detector concept is implemented in the c-quark tagging simulations. The detector consists of 5 CCD layers at 15, 26, 37, 48 and 60 mm. Figure 1 outlines the detector geometry.

Various visible energies in the detector are possible as determined by the mass difference between scalar top and neutralino. A small mass difference  $\Delta m$  corresponds to a small visible energy. Smaller mass differences are a larger challenge for the vertex detector as fewer and less energetic tracks are available to determine the quark flavor.

---

\*Presented at the 13th International Conference on Supersymmetry and Unification of Fundamental Interactions (SUSY’05), Durham, UK, July 18-23, 2005.

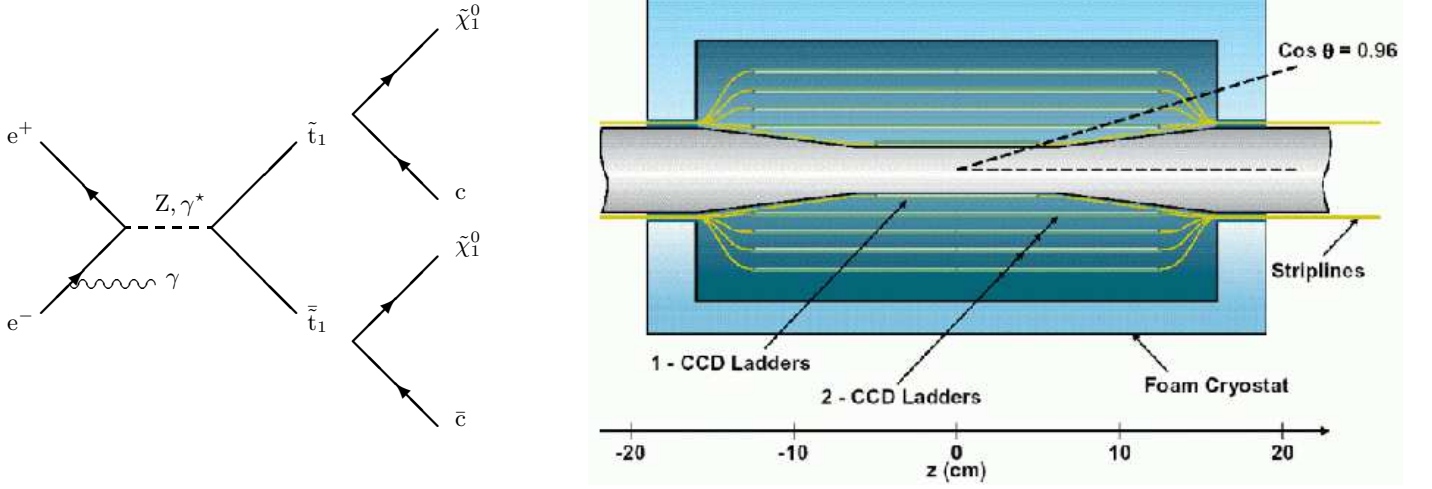


Figure 1: Left: scalar top production and decay. Right: illustration of the vertex detector with 5 CCD layers.

The work is presented as follows. First, detector simulations with SGV [3] and SIMDET [4] are compared for  $m_{\tilde{t}_1} = 180$  GeV and  $m_{\tilde{\chi}_1^0} = 100$  GeV. Then, also for large visible energy, the SPS-5 benchmark parameter point ( $m_{\tilde{t}_1} = 220.7$  GeV,  $m_{\tilde{\chi}_1^0} = 120.0$  GeV) has been studied. Different detector design variations are discussed, and four methods to determine the scalar top mass are compared. The experimental simulations of signal and background for small visible energy are presented and the scalar top mass and mixing parameter are determined for a scenario of the co-annihilation mechanism for Supersymmetric dark matter. Systematic and statistical uncertainties at a Linear Collider are discussed for a dark matter prediction. The expectation from different SUSY parameter combinations are compared with the current Cold Dark Matter (CDM) measurement.

## 2. SGV AND SIMDET COMPARISON FOR LARGE VISIBLE ENERGY

Signal and background events have been generated for  $\sqrt{s} = 500$  GeV and passed through the SIMDET 4.03 detector simulation. First, the 1000 fb $^{-1}$  simulation is compared to a previous SGV simulation in regard to signal efficiency and numbers of expected background events for  $m_{\tilde{t}_1} = 180$  GeV and  $m_{\tilde{\chi}_1^0} = 120$  GeV [5]:

Channel	SIMDET generated events	SIMDET preselection/500 fb $^{-1}$	previous SGV preselection/500 fb $^{-1}$
$c\tilde{\chi}_1^0\bar{c}\tilde{\chi}_1^0$	50 k	48%	47%
$q\bar{q}$	12169 k	64963	46788
$t\bar{t}$	620 k	32715	43759
$eeZ$	5740 k	24864	4069
$ZZ$	560 k	3100	4027
$W\ell\nu$	4859 k	252367	252189
$WW$	6800 k	122621	115243
Total background		500631	466075

The  $eeZ$  process has a lower expected rate in SGV, because of a different detector coverage in the forward-backward region. After additional cuts,  $E_{\text{vis}}/\sqrt{s} < 0.52$  and  $P_t/E_{\text{vis}} > 0.05$ , the following numbers of events are obtained:

Channel	$q\bar{q}$	$WW$	$W\ell\nu$	$t\bar{t}$	$ZZ$	$eeZ$	total
Background	6801	23278	226070	5267	125	2147	263691

The total number of background events agrees well with the previous 278377 events for the SGV simulation [6].

The signal to background ratio is optimized [6] by the IDA method [7]. First, by allowing a reduction of the signal of 50% most background events are removed. Without c-quark tagging 7815 (cf. SGV 7265) background events remain, while with c-quark tagging this number is reduced to 3600 events. Second, the IDA method is repeated. Figure 2 shows the background composition after IDA step 2 without c-quark tagging and the tagging performance after IDA step 1. For a 180 GeV signal and 12% detection efficiency, 680 (cf. SGV 400) background events remain without c-quark tagging, while with c-quark tagging 165 background events are expected.

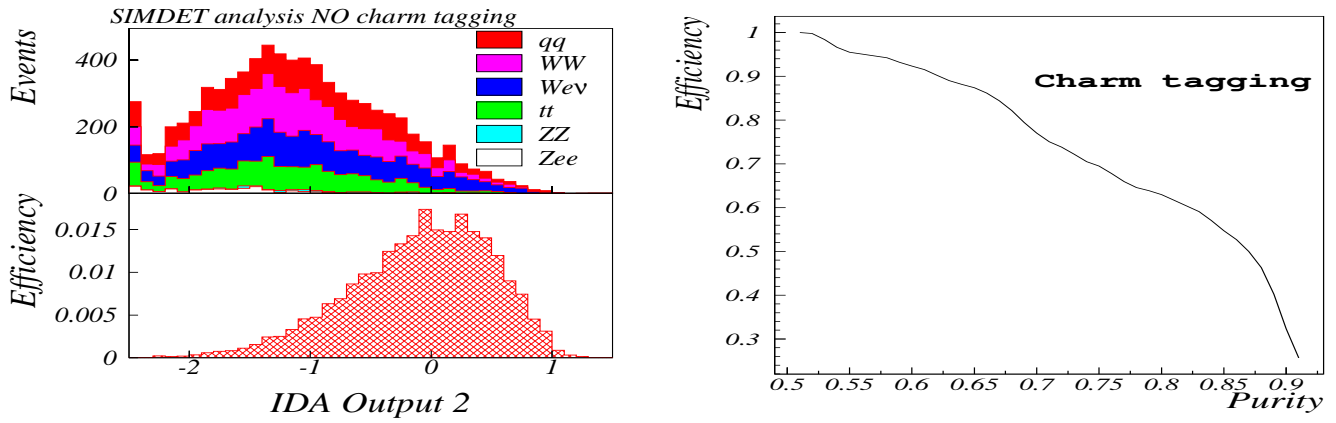


Figure 2: Left: IDA-2 output. Right: efficiency vs. purity of c-quark tagging after IDA step 1. Purity is defined as the ratio of the number of simulated signal events after the selection to all selected events.

### 3. SPS-5 (LARGE VISIBLE ENERGY): VERTEX DETECTOR DESIGN VARIATIONS

The development of a vertex detector for a Linear Collider is large challenge. A key aspect is the distance of the innermost layer to the interaction point, which is related to radiation hardness and beam background. Another key aspect is the material absorption length which determines the multiple scattering. The optimization of the vertex detector tagging performance is a further aspect. While at previous and current accelerators (e.g. SLC, LEP, Tevatron) b-quark tagging has revolutionized many searches and measurements, c-quark tagging will be very important at a future Linear Collider. Therefore, c-quark tagging could be a benchmark for vertex detector developments.

The analysis for a large mass difference with the SPS-5 parameter point (ISAJET)  $m_{\tilde{t}_1} = 220.7$  GeV,  $m_{\tilde{\chi}_1^0} = 120.0$  GeV and  $\cos\theta_{\tilde{t}} = 0.5377$  was previously performed [5]. For 25% (12%) efficiency 3800 (1800) signal events and 5400 (170) background events without c-quark tagging were obtained, while the background is reduced to 2300 (68) events with c-quark tagging.

The vertex detector absorption length is varied between normal thickness (TESLA TDR) and double thickness. In addition, the number of vertex detector layers is varied between 5 layers (innermost layer at 1.5 cm as in the TESLA TDR) and 4 layers (innermost layer at 2.6 cm). For SPS-5 parameters the following number of background events remain:

Thickness	layers	12% signal efficiency	25% signal efficiency
Single	5 (4)	68 (82)	2300 (2681)
Double	5 (4)	69 (92)	2332 (2765)

As a result, a significantly larger number of background events is expected if the first layer of the vertex detector is removed. The distance of the first layer to the interaction point is also an important aspect from the accelerator physics (beam delivery) perspective. The interplay between the beam delivery and vertex detector design in regard to critical tolerances like hardware damage of the first layer and occupancy (unable to use the data of the first layer) due to beam background goes beyond the scope of this study and will be addressed in the future.

No significant increase in the expected background is observed by doubling the thickness of the vertex detector layers. It is interesting to study this behavior for events with smaller visible energy in the detector, where a larger effect of the multiple scattering is expected. This study, based on the analysis in sec. 5, is in preparation [8].

### 4. SPS-5 (LARGE VISIBLE ENERGY): COMPARISON OF MASS DETERMINATIONS

The precision in the scalar top mass determination at a Linear Collider is crucial and four methods are compared for the SPS-5 parameter point [9]. Two of the methods rely on accurate cross section measurements, the other two use kinematic information from the observed jets. The signal events contain two charm jets with large missing energy from the unobserved  $\tilde{\chi}_1^0$ .

## 4.1. Mass Determination From Cross Section Measurements

Accurate cross section measurements combined with theoretical expectations will make it possible to obtain precise determinations of the scalar top mass. This requires a high signal sensitivity. An Iterative Discriminant Analysis (IDA) method [7] has been used to obtain a signal to background ratio of 10 or better. The expected size of the signal is between one thousand and two thousand events in  $500 \text{ fb}^{-1}$  luminosity at a Linear Collider with  $\sqrt{s} = 500 \text{ GeV}$  [6].

### 4.1.1. Use of beam polarization

A high degree of beam polarization is expected to be available at future  $e^+e^-$  colliders, and by measuring the production cross section in both left- and right-handed configurations,  $m_{\tilde{t}_1}$  and  $\cos\theta_{\tilde{t}}$  can be determined, as shown in Fig. 3 and discussed in Ref. [6, 10]. For  $2 \times 500 \text{ fb}^{-1}$  a precision of  $m_{\tilde{t}_1} = 220.7 \pm 0.57 \text{ GeV}$  and  $\cos\theta_{\tilde{t}} = 0.538 \pm 0.012$  is obtained.

### 4.1.2. Threshold scan

Measuring the cross section for scalar top production close to threshold and fitting a theoretical curve allows the mass to be deduced. The excitation curve near threshold has a  $\beta^3$  form. This is shown in Fig. 3 for six center-of-mass energies, each equivalent to a luminosity of  $50 \text{ fb}^{-1}$ . In this study the beam polarization  $P(e^-)/P(e^+) = +80\%/-60\%$  was assumed (right-handed  $e^-$ ) as this provides the best signal to background ratio, leading to  $m_{\tilde{t}_1} = 220.7 \pm 1.2 \text{ GeV}$ .

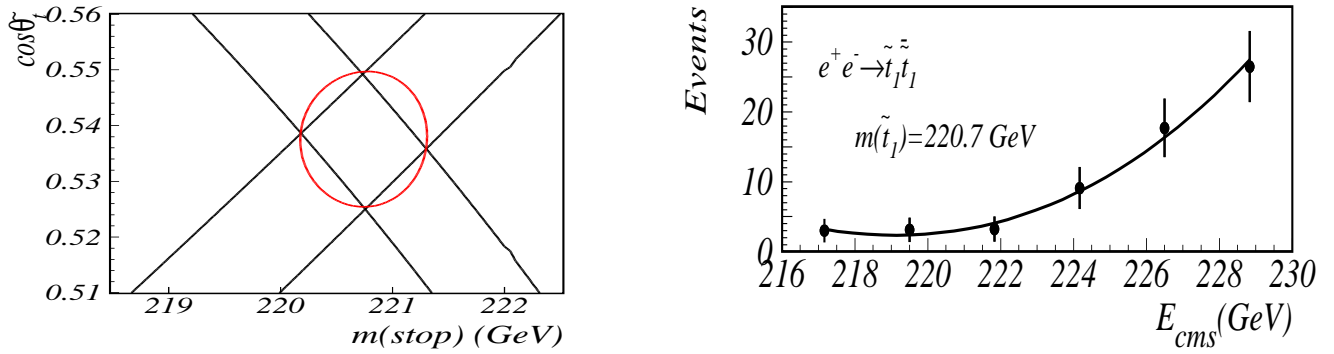


Figure 3: Left:  $m_{\tilde{t}_1}$  and  $\cos\theta_{\tilde{t}}$  determination from cross section measurements. The two bands correspond to different beam polarizations. The ellipse indicates the accuracy that could be obtained. Right: fit of the scalar top mass from cross section determination near threshold.

## 4.2. Mass Determination From Jet Measurements

The following two methods rely on measuring the kinematics of the observed jets, and thus deriving information about the originating quarks. The precision of this measurement depends on the jet energy resolution which is expected to be several GeV in this case as shown in Fig. 4.

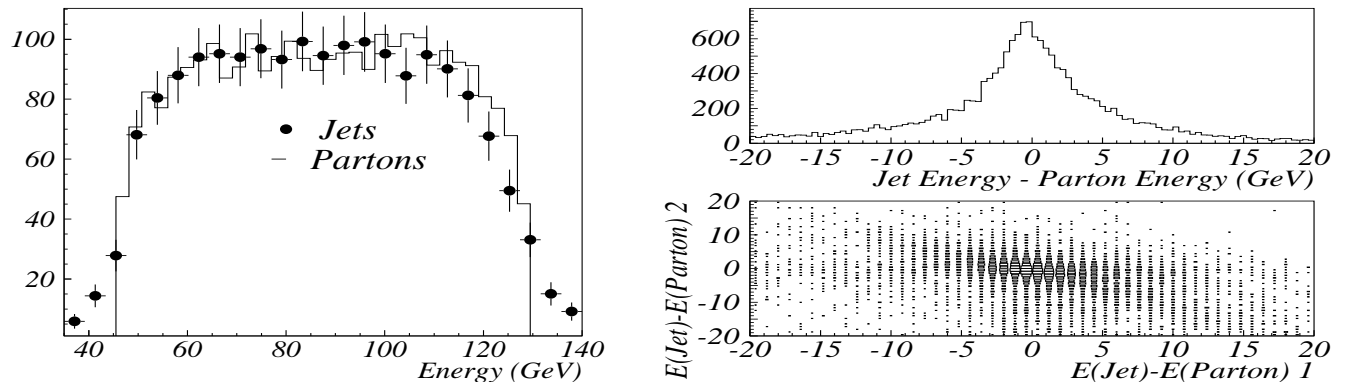
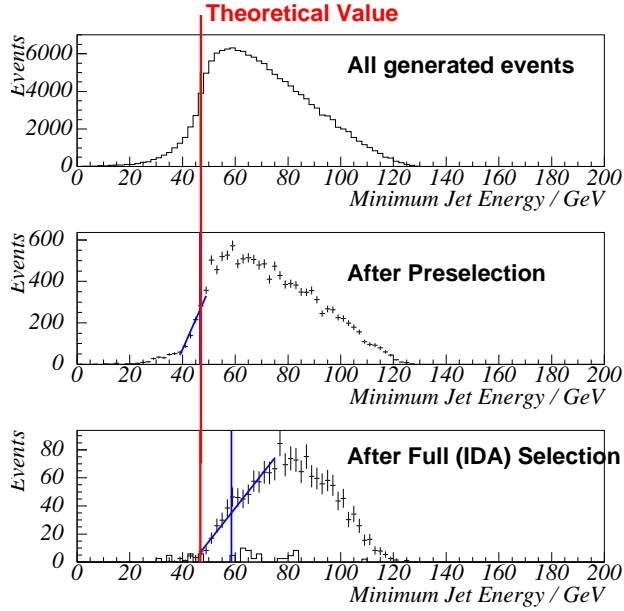


Figure 4: distributions of jet and parton energies.

The IDA method provides an optimal signal to background ratio, but distorts the jet energy measurements (Fig. 5), thus for this part of the analysis a simple cuts based selection is used. The cuts are also listed in the figure. About 900 signal events are selected (11% efficiency) and 390 background events remain (70% purity) for unpolarized beams.



Selection cuts:

- $20 < \text{number of energy flow objects} < 90$
- Visible energy  $< 0.8\sqrt{s}$
- Longitudinal momentum  $< 0.5$  visible energy
- Thrust  $< 0.95$
- Cosine of thrust axis relative to beam direction  $< 0.95$
- Both jet charm tags  $> 0.3$
- At least one jet charm tag  $> 0.4$
- Number of jets  $< 4$
- Lowest energy jet  $> 35$  GeV
- Highest energy jet  $< 140$  GeV

Figure 5: Left: distortion of minimum energy spectrum after IDA selection. Right: list of sequential selection cuts.

#### 4.2.1. End point method

The energy spectrum of a particle from a two-body decay is approximately a step function, whose end points contain information about the masses of both, the particle that decayed, and the other particle produced in the decay, which in this case is not observed. In the case of jets, this ideal situation is distorted by detector resolution, hadronization, and jet finding, as shown in Fig. 6. Several event samples are generated to obtain calibration curves and to determine the mass uncertainty.

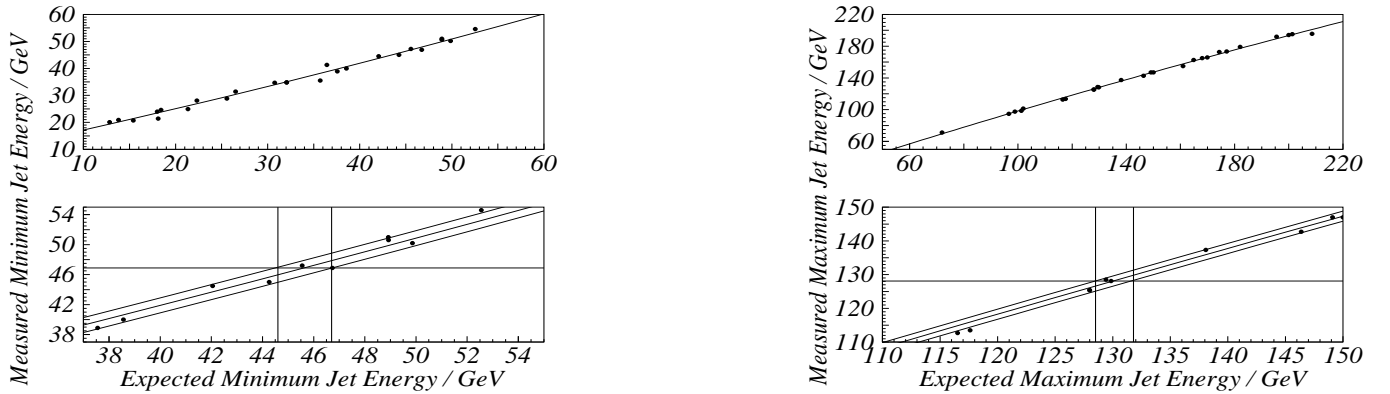


Figure 6: Minimum and maximum jet energy calibration for expected (parton) and simulated (jet) energies.

The precision for the minimum jet endpoint is  $45.7 \pm 1.0$  GeV, for the maximum jet endpoint  $130.2 \pm 1.5$  GeV, and the resulting masses are  $m_{\tilde{\tau}_1} = 219.3 \pm 1.7$  GeV and  $m_{\tilde{\chi}_1^0} = 119.4 \pm 1.6$  GeV.

#### 4.2.2. Minimum mass method

In the case when  $m_{\tilde{\chi}_1^0}$  is known, the minimum allowed mass of the two jets in an event can be calculated [11]. Figure 7 shows an example of the distribution of this variable. Fitting this distribution with a prediction from simulations allows a precise determination of  $m_{\tilde{\tau}_1}$ , as shown in Fig. 8. This method gives a precision of  $m_{\tilde{\tau}_1} = 220.5 \pm 1.5$  GeV.

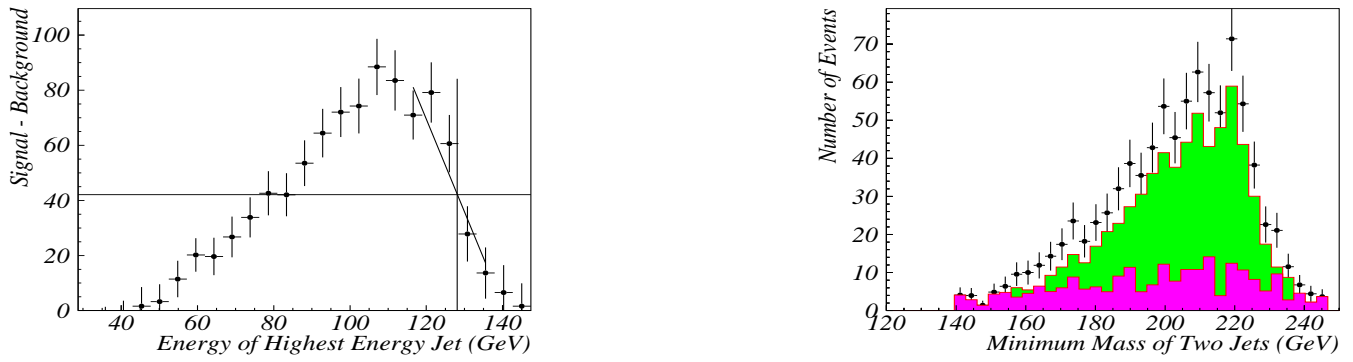


Figure 7: Examples of simulated maximum jet energy end points and the minimum mass of two jets. The points with error bars are the simulated signal. The light gray (green) histogram is the scalar top signal and the dark gray (magenta) histogram is the expected background.

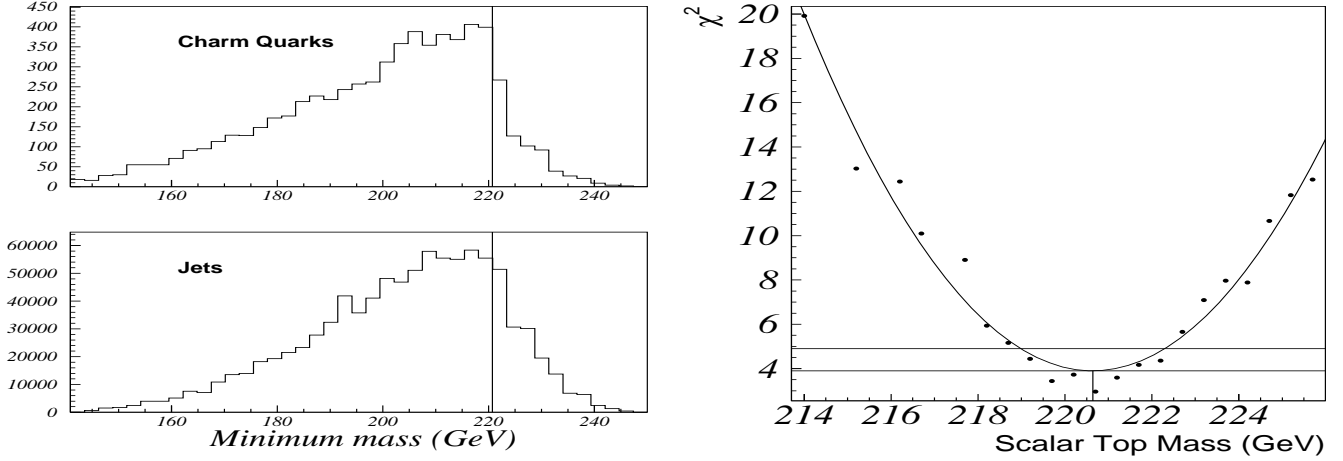


Figure 8: Left: minimum mass distribution for partons and jets. Right:  $\chi^2$  fit for different scalar top mass simulations.

### 4.3. Discussion of mass determinations

The precision of the mass determination of the four methods are summarized in Table I. Slightly higher precision is obtained from the polarization method, however, large theoretical uncertainties on the cross section calculations are not included. Overall a high sensitivity on the mass determination can be achieved.

Table I: Comparison of precision for scalar top mass determination

Method	$\Delta m$ (GeV)	luminosity	comment
Polarization	0.57	$2 \times 500 \text{ fb}^{-1}$	no theory errors included
Threshold scan	1.2	$300 \text{ fb}^{-1}$	right-handed $e^-$ polarization
End point	1.7	$500 \text{ fb}^{-1}$	
Minimum mass	1.5	$500 \text{ fb}^{-1}$	assumes $m_{\tilde{\chi}_1^0}$ known

## 5. SMALL VISIBLE ENERGY STUDIES

In this section, the production of light stops at a 500 GeV Linear Collider is analyzed, using high luminosity  $\mathcal{L} = 500 \text{ fb}^{-1}$  and polarization of both beams. The signature for stop pair production at an  $e^+e^-$  collider,

$$e^+e^- \rightarrow \tilde{t}_1 \bar{\tilde{t}}_1 \rightarrow c \tilde{\chi}_1^0 \bar{c} \tilde{\chi}_1^0, \quad (1)$$

is two charm jets and large missing energy. For small  $\Delta m$ , the jets are relatively soft and separation from backgrounds is very challenging. Backgrounds arising from various Standard Model processes can have cross sections that are several orders of magnitude larger than the signal, so that even small jet energy variations effects can be important. Thus, it is necessary to study also this process with a realistic detector simulation. Signal and background events



Table II: Cross sections for the stop signal and Standard Model background processes for  $\sqrt{s} = 500$  GeV and two polarization combinations. The signal is given for the stop mixing angle  $\cos\theta_{\tilde{t}} = 0.5$ . Negative/positive polarization values refer to left-/right-handed polarization, respectively.

Process	cross section [pb]		
$P(e^-)/P(e^+)$	0/0	-80%/+60%	+80%/-60%
$\tilde{t}_1\tilde{t}_1$ $m_{\tilde{t}_1} = 120$ GeV	0.115	0.153	0.187
$m_{\tilde{t}_1} = 140$ GeV	0.093	0.124	0.151
$m_{\tilde{t}_1} = 180$ GeV	0.049	0.065	0.079
$m_{\tilde{t}_1} = 220$ GeV	0.015	0.021	0.026
$W^+W^-$	8.55	24.54	0.77
$ZZ$	0.49	1.02	0.44
$We\nu$	6.14	10.57	1.82
$eeZ$	7.51	8.49	6.23
$q\bar{q}, q \neq t$	13.14	25.35	14.85
$t\bar{t}$	0.55	1.13	0.50
2-photon, $p_t > 5$ GeV	936	936	936

are generated with PYTHIA 6.129 [12], including a scalar top signal generation [13] previously used in Ref. [6]. The detector simulation is based on the fast simulation SIMDET [4], describing a typical ILC detector.

Table II lists the cross sections for the signal process and the relevant backgrounds. They have been computed with code used in Ref. [14] and by GRACE 2.0 [15], with cross checks to COMPHEP 4.4 [16]. A minimal transverse momentum cut,  $p_t > 5$  GeV, is applied for the two-photon background, to avoid the infrared divergence.

In the first step of the event selection, the following preselection cuts are applied:

$$\begin{aligned}
4 < N_{\text{charged tracks}} < 50, & \quad p_t > 5 \text{ GeV}, \\
|\cos\theta_{\text{Thrust}}| < 0.8, & \quad |p_{\text{long,tot}}/p_{\text{tot}}| < 0.9, \\
E_{\text{vis}} < 0.75\sqrt{s}, & \quad m_{\text{inv}} < 200 \text{ GeV}.
\end{aligned} \tag{2}$$

The cut on the number of charged tracks removes most leptonic background and part of the  $t\bar{t}$  background. By requiring a minimal transverse momentum  $p_t$ , the two-photon background and back-to-back processes like  $q\bar{q}$  are largely reduced. The signal is characterized by large missing energy and transverse momentum from the two neutralinos, whereas for most backgrounds the missing momentum occurs from particles lost in the beam pipe. Therefore, cuts on the thrust angle  $\theta_{\text{Thrust}}$ , the longitudinal momentum  $p_{\text{long,tot}}$ , the visible energy  $E_{\text{vis}}$  and the total invariant mass  $m_{\text{inv}}$  are effective on all backgrounds. The various background are substantially reduced after these preselection cuts, while about 70% of the signal is preserved, as shown in Table III.

After generating large event samples with the preselection cuts for the various backgrounds, as listed in Table III, the following final event selection cuts are applied to further improve the signal-to-background ratio:

1. Number of jets  $N_{\text{jets}} = 2$ . Jets are reconstructed with the Durham algorithm with the jet resolution parameter  $y_{\text{cut}} = 0.003 \times \sqrt{s}/E_{\text{vis}}$ . The cut reduces substantially the number of W and quark-pair events.
2. Large missing energy,  $E_{\text{vis}} < 0.4\sqrt{s}$ . This cut is effective against  $W^+W^-$ ,  $ZZ$  and di-quark events. In addition, a window for the invariant jet mass around the W-boson mass,  $70 < m_{\text{jet,inv}} < 90$  GeV, is excluded to reduce the large  $We\nu$  background.
3. The number of  $q\bar{q}$  events are reduced by requiring a minimal acollinearity angle  $\cos\phi_{\text{aco}} > -0.9$ .
4. Cutting on the thrust angle,  $|\cos\theta_{\text{Thrust}}| < 0.7$ , reduces W boson background.
5. A strong cut on the transverse momentum,  $p_t > 12$  GeV, completely removes the remaining two-photon events.
6. The largest remaining background is from  $e^+e^- \rightarrow We\nu$ . It resembles the signal closely in most distributions, e.g. as a function of the visible energy, thrust or acollinearity. By increasing the invariant jet mass window from cut 2 to ( $60 < m_{\text{jet,inv}} < 90$  GeV), the signal-to-background ratio is improved, but at the cost of a substantial signal reduction. In addition, the signal selection is enhanced by c-quark tagging, which is implemented based on the neural network analysis described in Ref. [17]. The neural network has been optimized to reduce the  $We\nu$  background while preserving the stop signal for small mass differences.

Table III: Left: background event numbers and  $\tilde{t}_1\bar{\tilde{t}}_1$  signal efficiencies (in %) for various  $m_{\tilde{t}_1}$  and  $\Delta m$  (in GeV) after preselection and each of the final selection cuts. In the last column the expected event number are scaled to a luminosity of  $500 \text{ fb}^{-1}$ . The cuts are explained in the text. Right: signal efficiencies (in %) for  $\tilde{t}_1\bar{\tilde{t}}_1$  production after final event selection for different combinations of the stop mass  $m_{\tilde{t}_1}$  and mass difference  $\Delta m = m_{\tilde{t}_1} - m_{\tilde{\chi}_1^0}$ .

Process	total	after presel.	cut 1	cut 2	cut 3	cut 4	cut 5	cut 6	scaled to 500 fb <sup>-1</sup>
W <sup>+</sup> W <sup>-</sup>	210,000	2814	827	28	25	14	14	8	145
ZZ	30,000	2681	1987	170	154	108	108	35	257
W e ν	210,000	53314	38616	4548	3787	1763	1743	345	5044
eeZ	210,000	51	24	20	11	6	3	2	36
q $\bar{q}$ , $q \neq t$	350,000	341	51	32	19	13	10	8	160
t $\bar{t}$	180,000	2163	72	40	32	26	26	25	38
2-photon	3.2 × 10 <sup>6</sup>	1499	1155	1140	144	101	0	0	< 164
$m_{\tilde{t}_1} = 140 :$									
$\Delta m = 20$	50,000	68.5	48.8	42.1	33.4	27.9	27.3	20.9	9720
$\Delta m = 40$	50,000	71.8	47.0	40.2	30.3	24.5	24.4	10.1	4700
$\Delta m = 80$	50,000	51.8	34.0	23.6	20.1	16.4	16.4	10.4	4840
$m_{\tilde{t}_1} = 180 :$									
$\Delta m = 20$	25,000	68.0	51.4	49.4	42.4	36.5	34.9	28.4	6960
$\Delta m = 40$	25,000	72.7	50.7	42.4	35.5	28.5	28.4	20.1	4925
$\Delta m = 80$	25,000	63.3	43.0	33.4	29.6	23.9	23.9	15.0	3675
$m_{\tilde{t}_1} = 220 :$									
$\Delta m = 20$	10,000	66.2	53.5	53.5	48.5	42.8	39.9	34.6	2600
$\Delta m = 40$	10,000	72.5	55.3	47.0	42.9	34.3	34.2	24.2	1815
$\Delta m = 80$	10,000	73.1	51.6	42.7	37.9	30.3	30.3	18.8	1410

$\Delta m$ (GeV)	$m_{\tilde{t}_1}$ (GeV)			
	120	140	180	220
80	10	15	19	
40	10	20	24	
20	17	21	28	35
10	19	20	19	35
5	2.5	1.1	0.3	0.1

The resulting event numbers, scaled to a luminosity of  $500 \text{ fb}^{-1}$ , and the signal efficiencies are listed in Table III. After the final selection, the  $\tilde{t}_1\bar{\tilde{t}}_1$  signal event numbers are of the same order as the remaining background,  $N \sim \mathcal{O}(10^4)$ .

To explore the reach for very small mass differences  $\Delta m = m_{\tilde{t}_1} - m_{\tilde{\chi}_1^0}$ , signal event samples have been generated also for  $\Delta m = 10 \text{ GeV}$  and  $5 \text{ GeV}$ , as shown in Fig. 9, together with results for larger mass differences. The signal efficiency drastically drops for  $\Delta m = 5 \text{ GeV}$  as a result of the  $p_t$  cut (cut 5). An optimization of the event selection for very small  $\Delta m$  will be addressed in future work.

Based on the above results from the experimental simulations, the discovery reach of a  $500 \text{ GeV } e^+e^-$  collider can be estimated (Fig. 9). The signal efficiencies for the parameter points in Fig. 9 are interpolated to cover the whole parameter region. The expected signal rates  $S$  are computed for each mass combination  $(m_{\tilde{t}_1}, m_{\tilde{\chi}_1^0})$ . Together with the number of background events  $B$ , this yields the significance  $S/\sqrt{S+B}$ . The gray (green) area in the figure corresponds to the  $5\sigma$  discovery region,  $S/\sqrt{S+B} > 5$ .

As evident from the figure, the ILC can find light stop quarks for mass differences down to  $\Delta m \sim \mathcal{O}(5 \text{ GeV})$ , beyond the stop-neutralino co-annihilation region. The figure (right plot) shows the reach which can be achieved with small total luminosities.

## 6. STOP PARAMETER DETERMINATION

The discovery of light stops would hint towards the possibility of electroweak baryogenesis and may allow the co-annihilation mechanism to be effective. In order to confirm this idea, the relevant Supersymmetry parameters need to be measured accurately. In this section, the experimental determination of the stop parameters will be discussed.

For definiteness, a specific MSSM parameter point is chosen:

$$\begin{aligned}
m_{\tilde{U}_3}^2 &= -99^2 \text{ GeV}^2, & A_t &= -1050 \text{ GeV}, & M_1 &= 112.6 \text{ GeV}, & |\mu| &= 320 \text{ GeV}, \\
m_{\tilde{Q}_3} &= 4200 \text{ GeV}, & \tan\beta &= 5, & M_2 &= 225 \text{ GeV}, & \phi_\mu &= 0.2.
\end{aligned} \tag{3}$$

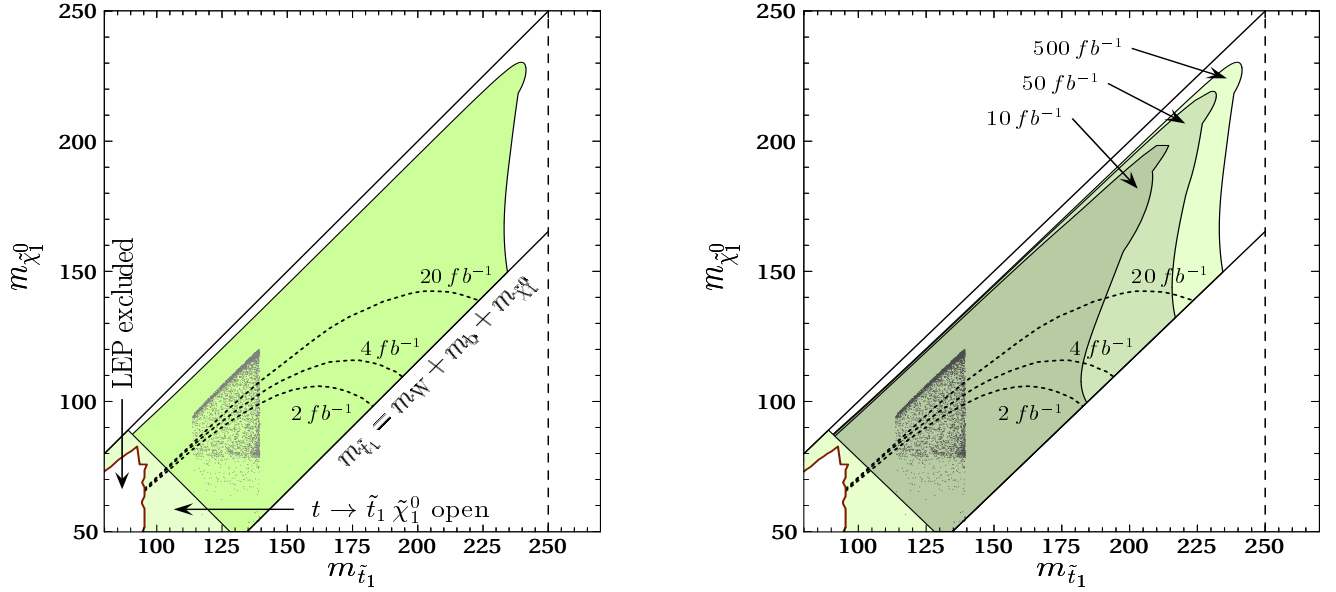


Figure 9: Left: discovery reach of a Linear Collider with  $500 \text{ fb}^{-1}$  luminosity at  $\sqrt{s} = 500 \text{ GeV}$  for the reaction  $e^+e^- \rightarrow \tilde{t}_1 \tilde{t}_1^* \rightarrow c\tilde{\chi}_1^0 \bar{c}\tilde{\chi}_1^0$ . The results are given in the stop vs. neutralino mass plane. In the gray shaded region, a  $5\sigma$  discovery is possible. The region  $m_{\tilde{\chi}_1^0} > m_{\tilde{t}_1}$  is inconsistent with a neutralino as Lightest Supersymmetric Particle (LSP), while for  $m_{\tilde{t}_1} > m_W + m_b + m_{\tilde{\chi}_1^0}$  the three-body decay  $\tilde{t}_1 \rightarrow W^+ \bar{b} \tilde{\chi}_1^0$  becomes accessible and dominant. In the light shaded corner to the lower left, the decay of the top quark into a light stop and neutralino is open. The dark gray dots indicate the region consistent with baryogenesis and dark matter. Also shown are the parameter region excluded by LEP searches [18] (white area in the lower left corner) and the Tevatron light stop reach [19] (dotted lines) for various integrated luminosities. Right: discovery reach for different luminosities.

The chosen parameters are compatible with the mechanism of electroweak baryogenesis, generating the baryon asymmetry through the phase of  $\mu$ . They correspond to a value for the dark matter relic abundance within the WMAP bounds,  $\Omega_{\text{CDM}} h^2 = 0.1122$ . The relic dark matter density has been computed with the code used in Ref. [20]. In this scenario, the stop and lightest neutralino masses are  $m_{\tilde{t}_1} = 122.5 \text{ GeV}$  and  $m_{\tilde{\chi}_1^0} = 107.2 \text{ GeV}$ , and the stop mixing angle is  $\cos \theta_{\tilde{t}} = 0.0105$ , i.e. the light stop is almost completely right-chiral. The mass difference  $\Delta m = m_{\tilde{t}_1} - m_{\tilde{\chi}_1^0} = 15.2 \text{ GeV}$  lies within the sensitivity range of the ILC.

The measurements of  $\tilde{t}_1 \tilde{t}_1^*$  production cross sections for different beam polarizations make it possible to extract both the mass of the light stop and the stop mixing angle [10]. Here it is assumed that  $250 \text{ fb}^{-1}$  is spent each for  $P(e^-)/P(e^+) = -80\%/+60\%$  and  $+80\%/-60\%$ , where negative/positive polarization degrees indicate left-/right-handed polarization. In the cross section measurements the statistical and systematic errors are similar and of about 0.8% each. A complete discussion of the systematic errors is given in Ref. [21].

Each of the two cross section measurements for  $P(e^-)/P(e^+) = -80\%/+60\%$  and  $+80\%/-60\%$  corresponds to a band in the parameter plane of the stop mass and mixing angle, as shown in Fig. 10. Combining the two cross section measurements, the stop parameter are determined to

$$m_{\tilde{t}_1} = 122.5 \pm 1.0 \text{ GeV}, \quad \cos \theta_{\tilde{t}} < 0.074 \quad \Rightarrow \quad \sin \theta_{\tilde{t}} > 0.9972. \quad (4)$$

The mass of the heavier stop  $\tilde{t}_2$  is too large to be measured directly, but it is assumed that a limit of  $m_{\tilde{t}_2} > 1000 \text{ GeV}$  can be set from collider searches. Combining the stop parameter measurements with corresponding data from the neutralino and chargino sector [21] makes it possible to compute the neutralino dark matter abundance from experimental results in the MSSM. All experimental errors are propagated and correlations are taken into account by means of a  $\chi^2$  analysis. The result of a scan over 100000 random points in the parameter space allowed by the expected experimental uncertainties for the scenario eq. (3) is shown in Fig. 10 as a function of the scalar top quark mass. The horizontal bands depict the relic density as measured by WMAP [1], which is at the  $1\sigma$  level  $0.104 < \Omega_{\text{CDM}} h^2 < 0.121$ . Further scenarios are investigated and compared to the WMAP measurement (Fig. 11).

The collider measurements of the stop and chargino/neutralino parameters constrain the relic density to  $0.100 < \Omega_{\text{CDM}} h^2 < 0.124$  at the  $1\sigma$  level, with an overall precision comparable to the direct WMAP determination.

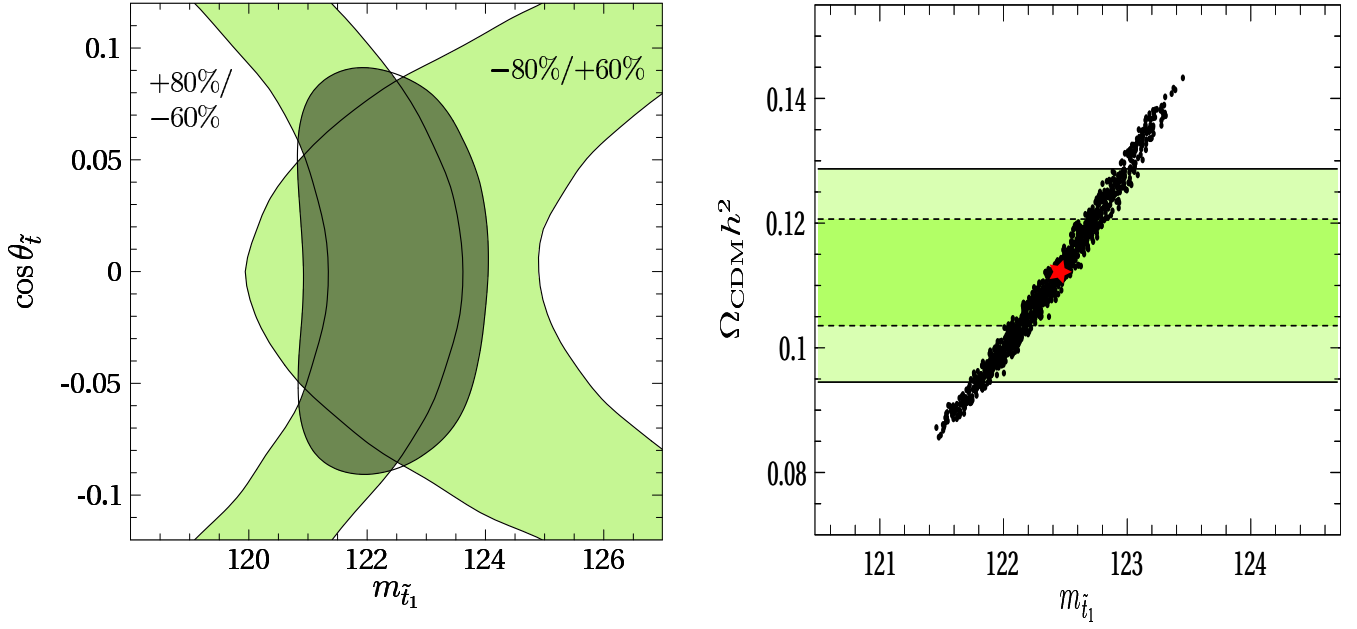


Figure 10: Left: determination of light stop mass  $m_{\tilde{t}_1}$  and stop mixing angle  $\theta_{\tilde{t}}$  from measurements of the cross section  $\sigma(e^+e^- \rightarrow \tilde{t}_1\tilde{t}_1)$  for beam polarizations  $P(e^-)/P(e^+) = -80\%/+60\%$  and  $+80\%/-60\%$ . Statistical and systematic errors are included. Right: computation of dark matter relic abundance  $\Omega_{\text{CDM}}h^2$  taking into account estimated experimental errors for stop, chargino, neutralino sector measurements at future colliders. The black dots correspond to a scan over the  $1\sigma$  ( $\Delta\chi^2 \leq 1$ ) region which is allowed by the expected experimental errors, as a function of the measured stop mass. The red star indicates the best-fit point. The horizontal shaded bands show the  $1\sigma$  and  $2\sigma$  constraints on the relic density measured by WMAP.

	A	B	C	D	E	F
$m_{\tilde{U}_3}^2$ [GeV <sup>2</sup> ]	-99 <sup>2</sup>	-99 <sup>2</sup>	-99 <sup>2</sup>	-97 <sup>2</sup>	-90.5 <sup>2</sup>	-85.5 <sup>2</sup>
$m_{\tilde{Q}_3}$ [GeV]	2700	3700	4200	4900	4700	4300
$A_t$ [GeV]	-860	-1150	-1050	-500	-400	0
$M_1$ [GeV]	107.15	111.6	112.6	119.0	123.2	129.0
$\tan \beta$	5.2	4	5	6	5.5	5.5
$A_{e,\mu,\tau} \times e^{i\pi/2}$	5	3.7	5	5.8	5.2	5
$m_{\tilde{t}_1}$ [GeV]	117.1	118.0	122.5	130.2	135.2	139.4
$m_{\tilde{\chi}_1^0}$ [GeV]	102.1	104.1	107.2	114.0	118.1	123.1
$\cos \theta_{\tilde{t}}$	0.0210	0.0150	0.0105	0.0038	0.0035	0.0005
$m_{h^0}$ [GeV]	115.1	115.0	117.0	117.1	116.2	115.1
$\Omega_{\text{CDM}}h^2$	0.113	0.060	0.112	0.144	0.166	0.112

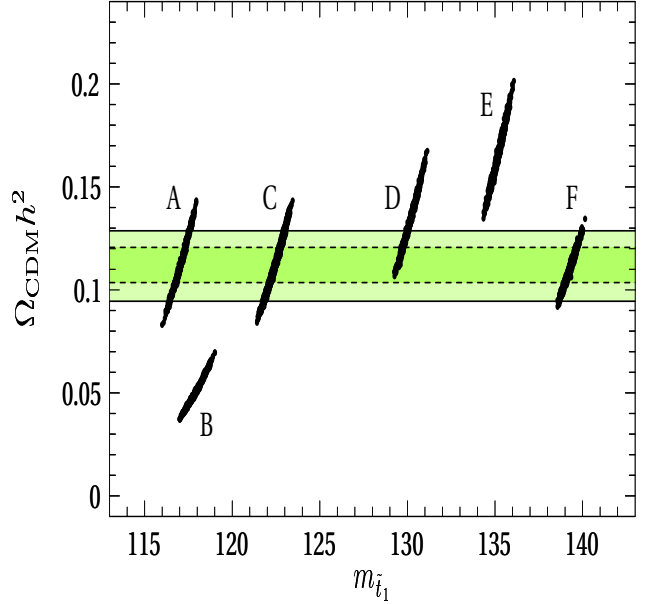


Figure 11: Left: dark matter scenarios in the Supersymmetric model. Point C corresponds to the scenario discussed before. Right: dark matter relic abundance  $\Omega_{\text{CDM}}h^2$  for WMAP  $1\sigma$  and  $2\sigma$  error bands and expected Linear Collider precision for benchmarks A-F.

## 7. CONCLUSIONS

Scalar top quark production and decay at a Linear Collider are studied with a realistic detector simulation with focus on the c-tagging performance of a CCD vertex detector. The SIMDET simulation largely agrees with the previous SGV simulation in the kinematic distributions. In addition, the SIMDET simulation includes a CCD vertex detector (LCFI Collaboration). The tagging of c-quarks reduces the background by about a factor 3 in the  $c\tilde{\chi}_1^0\bar{c}\tilde{\chi}_1^0$  channel. Thus, scalar top processes can serve well as a benchmark reaction for the vertex detector performance.

Dedicated simulations with SPS-5 parameters are performed. The expected background depends significantly on the detector design, mostly on the radius of the inner layer. Future studies of different detector designs will include simulations with small scalar top and neutralino mass differences.

For the scalar top mass determination four methods are compared. The polarization method gives the highest precision. The other methods are also important as they contribute to the determination of the properties of the scalar top quark. For example, the scalar character of the stops can be established from the threshold cross section scan.

A new study for small mass difference, thus small visible energy, shows that a Linear Collider has a large potential to study the scalar top production and decay, in particular in this experimentally very challenging scenario.

From detailed simulations together with estimated errors for measurements in the neutralino/chargino sector, the expected cosmological dark matter relic density can be computed. The precision at a Linear Collider will be similar to the current precision of WMAP. The uncertainty in the dark matter prediction from a Linear Collider is dominated by the precision of the scalar top quark mass measurement.

## Acknowledgments

The authors are grateful to P. Bechtle, S. Mrenna and T. Kuhl for practical advice.

## References

- [1] D. N. Spergel *et al.* [WMAP Collaboration], *Astrophys. J. Suppl.* **148**, 175 (2003); M. Tegmark *et al.* [SDSS Collaboration], *Phys. Rev. D* **69**, 103501 (2004).
- [2] C. Balázs, M. Carena and C. E. M. Wagner, *Phys. Rev. D* **70**, 015007 (2004).
- [3] M. Berggren, Simulation Grand Vitesse (SGV), <http://berggren.home.cern.ch/berggren/sgv.html>.
- [4] M. Pohl and H. J. Schreiber, hep-ex/0206009.
- [5] A. Finch, H. Nowak and A. Sopczak, “CCD Vertex Detector Charm-Tagging Performance in Studies of Scalar Top Quark Decays”, *Proc. of the International Conference on Linear Colliders (LCWS 04)*, Paris, France, 19-24 April 2004.
- [6] A. Finch, H. Nowak and A. Sopczak, contributed paper EPS370, *Int. Conference on High-Energy Physics (HEP 2003)*, Aachen, Germany, 17-23 July 2003 [LC Note LC-PHSM-2003-075].
- [7] J. Malmgren and K. Johansson, *Nucl. Inst. Methods A* **403** (1998) 481.
- [8] C. Milstène and A. Sopczak, “LCFI Vertex Detector Design Studies”, in preparation.
- [9] A. Finch, H. Nowak and A. Sopczak, “Determination of the Scalar Top Mass at a Linear  $e^+e^-$  Collider”, *Proc. of the International Conference on Linear Colliders (LCWS’04)*, Paris, France, 19-24 April 2004.
- [10] A. Bartl, H. Eberl, S. Kraml, W. Majerotto, W. Porod and A. Sopczak, *Z. Phys. C* **76**, 549 (1997).
- [11] J. Feng and D. Finnell, *Phys. Rev. D* **49** (1994) 2369.
- [12] T. Sjöstrand *et al.*, *Comput. Phys. Commun.* **135**, 238 (2001).
- [13] A. Sopczak, in *PHYSICS AT LEP2*, “Event Generators for Discovery Physics”, CERN Yellow Report CERN 96-01.
- [14] A. Freitas, D. J. Miller and P. M. Zerwas, *Eur. Phys. J. C* **21** (2001) 361;  
A. Freitas, A. von Manteuffel and P. M. Zerwas, *Eur. Phys. J. C* **34** (2004) 487.
- [15] F. Yuasa *et al.*, *Prog. Theor. Phys. Suppl.* **138**, 18 (2000).
- [16] E. Boos *et al.* [CompHEP Collaboration], *Nucl. Instrum. Meth. A* **534**, 250 (2004).
- [17] T. Kuhl, “Hadronic branching ratio of a SM-like Higgs boson at a future linear collider”, *Proc. of the International Conference on Linear Colliders (LCWS 04)*, Paris, France, 19-24 April 2004.
- [18] LEP2 SUSY Working Group, ALEPH, DELPHI, L3 and OPAL experiments, note LEPSUSYWG/04-02.1.
- [19] R. Demina, J. D. Lykken, K. T. Matchev and A. Nomerotski, *Phys. Rev. D* **62**, 035011 (2000).
- [20] C. Balázs, M. Carena, A. Menon, D. E. Morrissey and C. E. M. Wagner, *Phys. Rev. D* **71**, 075002 (2005).
- [21] M. Carena, A. Finch, A. Freitas, C. Milstène, H. Nowak and A. Sopczak, hep-ph/0508152, accepted for publication in *Phys. Rev. D*.